Spatially-variant B_0 field gradients in the liver: implications for R_2* mapping for iron quantification

Debra E. Horng[1,2], Diego Hernando[1], Jens-Peter Kühn[1,3], and Scott B. Reeder[1,2]

[1]*Radiology, University of Wisconsin-Madison, Madison, WI, United States,* [2]*Medical Physics, University of Wisconsin-Madison, Madison, WI, United States,*
[3]*Radiology and Neuroradiology, Ernst Moritz Arndt University Greifswald, Greifswald, Germany*

Introduction: R_2* relaxometry is a promising technique for liver iron quantification[1]. However, measured R_2* values are affected by several confounding factors, including the presence of macroscopic B_0 field inhomogeneities due to susceptibility effects, e.g., near the dome of the liver (Fig. 1). Susceptibility effects introduce errors in the apparent R_2*, and these errors can be highly protocol-dependent. The purpose of this work is to characterize the B_0 distribution in the liver in order to optimize acquisition strategies.

Methods: After IRB approval, 6 patients with no known iron overload underwent chemical shift-based MR imaging of the liver acquired at 3T using an investigational multi-echo 3D spoiled gradient echo, with two protocols with different image parameters. ***Protocol 1:*** sagittal slab, TR=9.0 ms, 6 echoes/TR (1 shot), TE_1=0.8 ms, ΔTE=1.2 ms, with slice thickness = 3.0 mm. ***Protocol 2:*** axial slab, TR=8.0 ms, 3 echoes/TR (2 shots), TE_1=1.2 ms, ΔTE=1.0 ms, with slice thickness = 8.0 mm. Separated water and fat images, an R_2* map, and a B_0 field map were obtained using a chemical shift-based water-fat separation algorithm[2]. The spatial gradient of the B_0 field map (in $\hat{x}$, $\hat{y}$, $\hat{z}$) was computed from the sagittal data. ROIs were placed in the 9 Couinaud segments of the liver by a radiologist with >5 years experience in liver imaging, in order to measure the 3 components of the gradient. Theoretical B_0 field maps were calculated[3] for each subject based on known susceptibility values of water/fat/air[4], and an anatomically specific susceptibility distribution (derived from the fat-water separation described above), in order to characterize the source of B_0 field inhomogeneities. Finally, theoretical B_0 gradients were obtained from the calculated B_0 field for each segment in each subject, and compared with the measured B_0 field gradients.

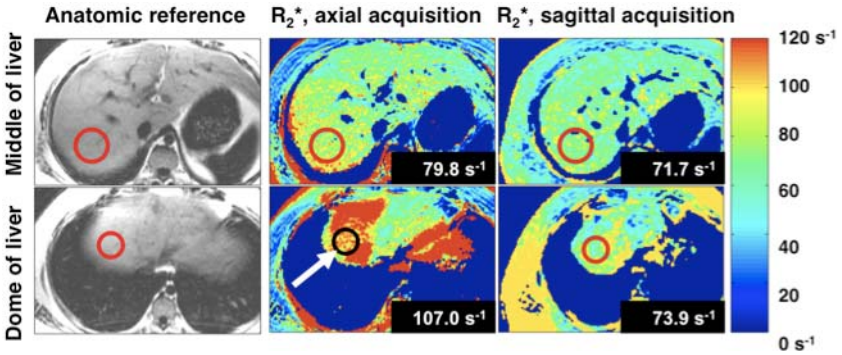

Figure 1. Apparent R_2* values are protocol-dependent. Axial acquisition at the dome (white arrow) shows increased R_2* (107.0 s^{-1}, σ=12.4 s^{-1}) relative to sagittal at the dome (73.9 s^{-1}, σ=15.5 s^{-1}). R_2* in the sagittal acquisition at the dome is closer to both the axial at the middle (79.8 s^{-1}, σ=12.4 s^{-1}) and the sagittal acquisition at the middle (71.7 s^{-1}, σ=10.4 s^{-1}).

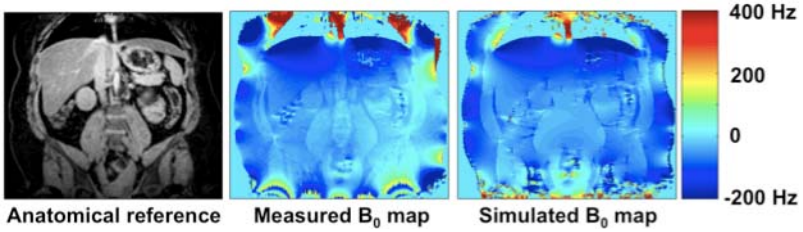

Figure 2. Coronal views of a water image, the measured B_0 map, and the simulated B_0 map.

Results: Segment 2 has the highest gradients with an average of 22.0 Hz/cm for the measured gradients, and also the highest standard deviation at an average of ±13.6 Hz/cm (Fig. 3). Segments 4A, 7, and 8 also have large gradients in the $\hat{z}$ direction (all above 15 Hz/cm). The measured and simulated average gradients have correlations of 0.79 for $\hat{x}$, 0.91 for $\hat{y}$, and 0.83 for $\hat{z}$, demonstrating good agreement. In contrast to the agreement between theoretical and measured average gradients in Fig. 3, Fig. 4 demonstrates that the simulated gradients do not predict the measured gradients well for an individual segment of a particular liver.

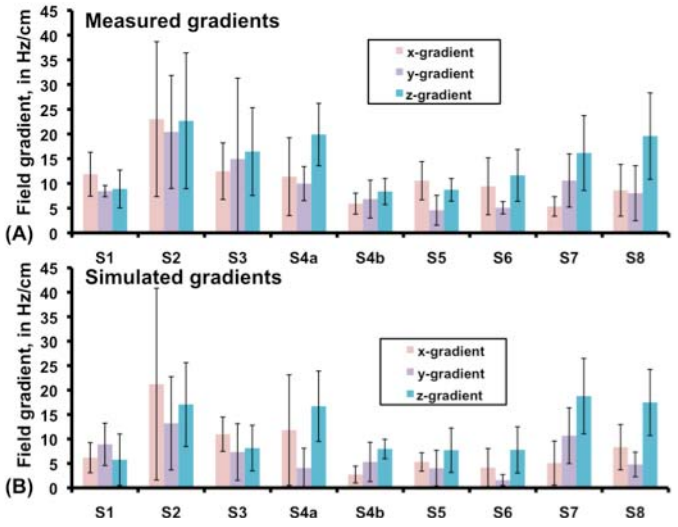

Figure 3. On average, the behavior of the measured and simulated B_0 gradients appears very similar. Gradients are measured (a) and simulated (b) for each segment of the liver, for $\hat{x}$, $\hat{y}$, and $\hat{z}$.

Discussion and Conclusion: The difference in the behavior between the average gradients in Fig. 3 and the individual gradients in Fig. 4 may be explained by the relative simplicity of the susceptibility model used in the simulation. Rapid field variations along $\hat{z}$ near the liver dome (segments 4A, 7, 8) result in an increase in the apparent R_2*, as often observed in scans acquired axially with thick slices. ***Thus, sagittal or coronal acquisitions, rather than axial, may be preferable if localized R_2* measures near the liver dome are required.*** The methods presented in this work may be used to optimize acquisition parameters to minimize the field variation within a voxel to avoid susceptibility-related errors in R_2* measurement for liver iron quantification.

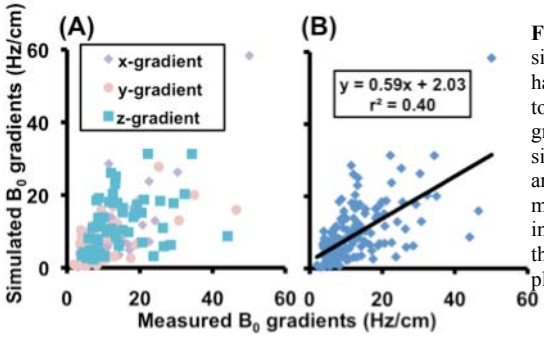

Figure 4. Individual simulated gradients have limited ability to predict individual gradients. The simulated gradients are plotted against measured gradients in $\hat{x}$, $\hat{y}$, and $\hat{z}$ (a), and the magnitudes are plotted in (b).

References: **1.** Wood J *et al*. Blood. 106(4):1460-5. **2.** Yu H *et al*. MRM. 26(4):1153-61. **3.** Koch KM *et al*. Phys Med Biol. 51(24):6381-402. **4.** Collins CM *et al*. MRI. 20(5):413-24.

Acknowledgements: We gratefully acknowledge support from the NIH (R01 DK083380, R01 DK088925, and RC1 EB010384), WARF Accelerator Program, the Coulter Foundation, and GE Healthcare.